

Radon Emanation from Dust of Varying Composition and Size

Yue Meng^{a,b,c,*}, Jerry Busenitz^a, Andreas Piepke^a, Raymond Tsang^a,
Mengmeng Wu^d, Yukun Yao^b

^a*Department of Physics and Astronomy, University of Alabama, Tuscaloosa, AL 35487, US*

^b*School of Physics and Astronomy, Shanghai Jiao Tong University, MOE Key Laboratory for Particle Astrophysics and Cosmology, Shanghai Key Laboratory for Particle Physics and Cosmology, Shanghai 200240, China*

^c*Shanghai Jiao Tong University Sichuan Research Institute, Chengdu 610213, China*

^d*School of Physics, Sun Yat-Sen University, Guangzhou 510275, China*

Abstract

^{222}Rn emanating from environmental dust constitutes an important background component for many low-energy, low-rate experiments. Radon emanation rates from dust and rock, thus, are important for experiment planning. In this paper, we report measured radon emanation fractions (defined here as the ratio of the transient to the total radon progeny activity of a sample) for five types of dust differing in grain size and composition. These data were obtained using high-purity germanium detectors (HPGe), measuring emanated and non-emanated ^{222}Rn progeny activities. The two components were distinguished by means of the temporal change of the measured activities. The range of observed radon emanation fractions ranges from $3.5 \pm 1.9\%$ and $16.1 \pm 0.84\%$. The impact of the water, contained in the dust, might have on the emanation fraction was evaluated and found to be small. The data presented here do not show a clear correlation between dust particle size and emanation fraction, as hypothesized when starting this study. Our measurement results are compared to expectations of radon emanation models.

Keywords: Radon Emanation, Dusts and Rocks, High Purity Germanium Detector(HPGe), Ultra-low Background Experiments

*mengyue@sjtu.edu.cn

1. Introduction

^{238}U is present in rock typically at ppm-concentrations, together with its progeny, decaying at equal rates. Because of its relatively long half-life, the low-reactivity noble gas ^{222}Rn ($T_{1/2}=3.8235$ d), one of the ^{238}U progeny, may remain in or exit its host material by means of diffusion or recoil. This process of radon outgassing is sometimes called emanation. Because of its low reactivity, emanated ^{222}Rn readily travels through gases and into experimental systems. The β and γ -radiation subsequently emitted in the decay of its daughters can then result in unwanted background signals. α -emitting radon daughters can further contribute neutron-induced background events via nuclear α -n-reactions on low-Z materials. Both sources of backgrounds - direct and induced emissions - constitute an important interference for rare-event searches such as dark matter and neutrinoless double-beta decay experiments [1, 2, 3, 4, 5, 6, 7, 8, 9, 10, 11, 12]. More generally, due primarily to the risks to human health from environmental radon, radon emanation from dust, rocks, soil, and building materials has been the subject of many investigations; see [13, 14, 15, 16] for examples and further references. Because of its relatively short half life of 55.6 s the ^{232}Th progeny ^{220}Rn is rarely a background concern. It converts quickly into its reactive progeny, thus, becoming immobile. The study presented here focuses on ^{222}Rn .

In soil, which typically exhibits U-chain secular equilibrium , the summed emanated and non-emanated ^{222}Rn activity equals that of its long-lived parent ^{226}Ra ($T_{1/2}=1600$ y). The emanated ^{222}Rn fraction can be measured by observing the in-growth of its daughters ^{214}Pb and ^{214}Bi . This can be done after initially removing the radon gas from a sample, thus allowing to observe how it grows back. Such removal leaves the non-emanated ^{222}Rn fraction, and with the activities of its daughters, unchanged. It is known from the literature that the radon diffusion constants in intact dust grains are exceedingly small [17], leading to diffusion lengths much shorter than typical ion recoil ranges. In such situation ^{222}Rn release is mainly driven by nuclear recoil and one would not

expect a strong temperature dependence. For the study presented here, all measurements were, therefore, performed at room temperature. The possible impact of moisture may warrant future studies of this point.

In this study, γ -spectroscopy is utilized to determine the decay rates of ^{226}Ra , ^{214}Pb and ^{214}Bi . The ^{226}Ra decay rate is expected to stay constant, serving as a convenient monitor. The observed time dependence of the ^{214}Pb and ^{214}Bi decay rates allows us to infer both the emanated and non-emanated radon fractions. The ^{226}Ra decay rate was determined using the 186 keV γ -peak. The ^{214}Pb and ^{214}Bi decay rates were derived from their prominent γ -peaks at 295 keV and 352 keV (^{214}Pb), and 609 keV, 1120 keV and 1764 keV (^{214}Bi).

2. Sample Characteristics

Measurements with five dust samples are reported in this paper. Four were procured commercially¹. These commercial samples came with certificates of analysis for grain size and composition. They were chosen to explore radon emanation for a range of compositions and grain sizes; further, for some of these samples, measurements may be found in the literature on grain shape and texture, which are also useful for modeling. The choice of grain size distributions was guided by the availability of commercial, pre-characterized samples. The study presented here is limited to a phenomenological approach. While simple modelling has been attempted and is described below, an exhaustive study of all possible parameters impacting radon emanation was beyond the scope of this work. The samples and their characteristics, such as average particle size and size distribution, are listed in Table 1. Samples A1 and A4, varieties of so-called Arizona test dust, have the same chemical composition but exhibit different grain size distributions. Compared to samples A1 and A4, samples AFRL-02 and AFRL-03 have a different chemical composition. Compared to each other,

¹Powder Technology Inc., www.powdertechnologyinc.com

samples AFRL-02 and AFRL-03 have identical chemical compositions but show different median grain sizes of their quartz components.

The sample densities were estimated in our laboratory and served as input to the detector simulation code. The effective dust density relies on a geometrical estimation of the sample volume. We estimate the uncertainty of this quantity to be $\pm 10\%$. The fifth sample is comprised of dust collected by a HEPA vacuum in the underground cleanroom at the Sanford Underground Research Facility (SURF) and includes household waste. Larger debris was separated from the finer, more dust-like component, before performing measurements.

Sample	Composition	Mass [g]	Average Density [g/cm ³]	Particle Size Average/Standard Deviation [μm]
A1 Ultrafine	1-4% Sodium oxide 4-7% Iron(III) oxide 1-2% Magnesium oxide 0-1% Titanium dioxide	103.1	0.70	5.3/3.3
A4 Coarse	69-77% Silica 8-14% Aluminium oxide 2.5-5.5% Calcium oxide 2-5% Potassium oxide	124.1	1.20	51/53
AFRL-02	34% Quartz 30% Gypsum 17% Aplite	295.7	0.59	18/21
AFRL-03	14% Dolomite 5% Salt	323.6	0.65	26/25
SURF SAL sweepings	unknown	163.4 (screened)	0.39	328/242

Table 1: Characteristics of dust samples used in this study: chemical composition, density and average particle size. The average particle sizes and their variability were derived from the particle size distributions. The variability is, therefore, not a direct measure of uncertainty but a characteristic of the dust samples. Screened SURF SAL sweepings include dust component only.

The particle size distributions for the commercial samples, as supplied by the vendor, are shown in Figure 1a and 1b. Before determining particle size distribution of the SURF dust sample, shown in Figure 1c, it was filtered with a 1000 μm mesh sieve to separate debris from dust. The sample was then

Sample	% Mass Less Than	Quartz Grain Size [μm]	Gypsum Grain Size [μm]	Salt Grain Size [μm]
AFRL-02	10	1.0 ± 0.5	2.0 ± 1.0	1.0 ± 0.5
	50	4.0 ± 1.5	11.5 ± 2.0	2.00 ± 0.75
	90	8.5 ± 2.5	38.0 ± 3.0	4.0 ± 1.0
AFRL-03	10	5.0 ± 1.0	2.0 ± 1.0	1.0 ± 0.5
	50	24.0 ± 2.5	11.5 ± 2.0	2.00 ± 0.75
	90	51.0 ± 4.5	38.0 ± 3.0	4.0 ± 1.0

Table 2: Grain size distributions for the quartz, gypsum, and salt components of the AFRL dust samples. These components are blended with the dolomite (Dolocron 40-13) and aplite (Minspar 200) components after the dolomite and aplite have been sieved with a minus 200 mesh. Different components remain different grains.

measured by Bettersize Instruments Ltd. in China². As a further cross check of the size assessment, samples of A1 and A4 dust were submitted to Bettersize Instruments Ltd. for analysis. The size distributions obtained by them were found to be in qualitative agreement with the vendor data.

Concerning the shape and texture of the grains, measurements have been reported for Arizona test dust samples derived from the same feedstock and overlapping in grain size with the Arizona test dust samples investigated in this work. In one investigation [18], the aspect ratio (L/W), projected diameter, longest chord, and circularity were measured from SEM images. The measurements of aspect ratio and circularity show clear—but not extreme—deviations from symmetry and the edges of the two-dimensional images appear smooth. A second work [19] used SEM and atomic force microscopy (AFM) to measure grain shape and texture. The grains were found to be smooth within the resolution of the measurement methods and to be approximated in shape by oblate spheroids where the equatorial diameter exceeded the polar diameter by an order of magnitude on average. The specific area, which depends on the surface/volume ratio and surface texture, was estimated to be $4.4 \text{ m}^2/\text{g}$, which may be compared to another result of $5.7 \text{ m}^2/\text{g}$ [20] based on Brunauer–Emmett–

²Bettersize Instruments Ltd, <https://www.bettersizeinstruments.com>

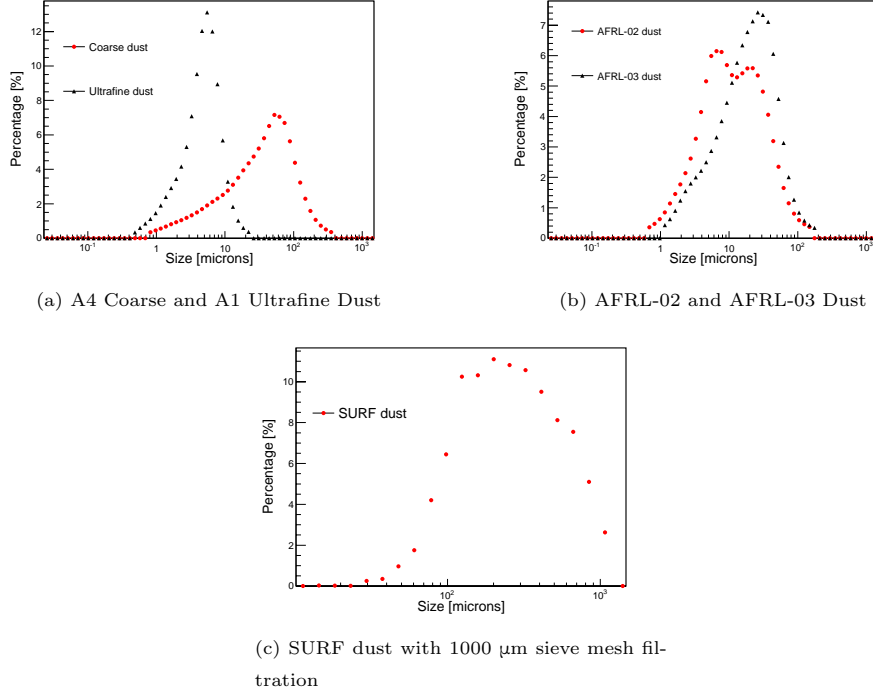


Figure 1: Particle size (principal axis) distributions of dust samples

Teller theory (BET). A third paper [21] reported the results of measuring the Corey shape factor (CSF), which depends on the lengths of a grain along 3 orthogonal axes via

$$\text{CSF} \equiv \frac{d_{\min}}{\sqrt{d_{\max}d_{\text{med}}}}$$

The CSF values for all grains measured fell in the range 0.1-0.95 with a mean and standard deviation of 0.55 and 0.20, respectively. All three studies found that the shape factors do not depend strongly on grain size. The results of all three studies indicate that the dust grains shapes cannot, as a rule, be approximated as spheres, although it is difficult to judge the quantitative consistency between the three studies as each measured different shape characteristics. To our knowledge, shape measurements have not been reported in the literature for the AFRL samples.

3. Procedure

To investigate a possible relation between the radon emanation fraction and average particle size or composition, the following measurement procedure was followed for all samples. The sample was spread out in a thin layer, facilitating ventilation of captured radon. The sample was ventilated in a fume hood with ambient air for a few days. All emanated radon is presumed to escape in this process. The sample was then tightly wrapped and sealed into a Mylar bag of 0.05 mm thickness. The Mylar bags are excellent radon barriers [22], prohibiting radon atoms to escape to any significant degree. Without further delay, the sealed sample was placed in one of two shielded low-background HPGe detector setups utilized in this study. Samples were counted for a period of 10–14 days. The impact of this small variation of the water content of the A4 sample was found to be small, as shown in Table 3. A larger water content could well result in a larger impact.

The dust samples as received for our measurements were dry. During the first step of the procedure, however, in which the radon was vented, the dust was exposed to laboratory air in which the relative humidity varied in the range 30–50%. To investigate whether or not this introduced a systematic effect in our measurement results due to significant absorption of water by the dust samples, the first sample was dried by pumping and baking for 24 h at 200 °C. The sample was collected and sealed into double 0.1 mm Nylon bags. As shown in [22], Nylon is good radon barrier too. A second sample of A4 dust was exposed to moist air (relative humidity ~70%) for 24 h and also sealed in double Nylon bags. Both samples were then counted ~10 days.

Sample counting utilized two different shielded low background Ge detector setups.

- Most sample counting was performed with the above-ground UA GeII setup, operated at the University of Alabama (UA). The setup consist

of a low background Canberra p-type coaxial germanium detector with copper and lead shielding. Large Bicron plastic scintillation panels are utilized as active muon veto system.

- The de-watering studies, as well as comparative measurements with the A4 sample, were performed with the JP Ge2 setup, located in the Jinping underground laboratory in China. The setup utilizes a low background Canberra germanium detector and is equipped with a copper and lead passive radiation shield. 2400 m of rock provide cosmic rays shielding.

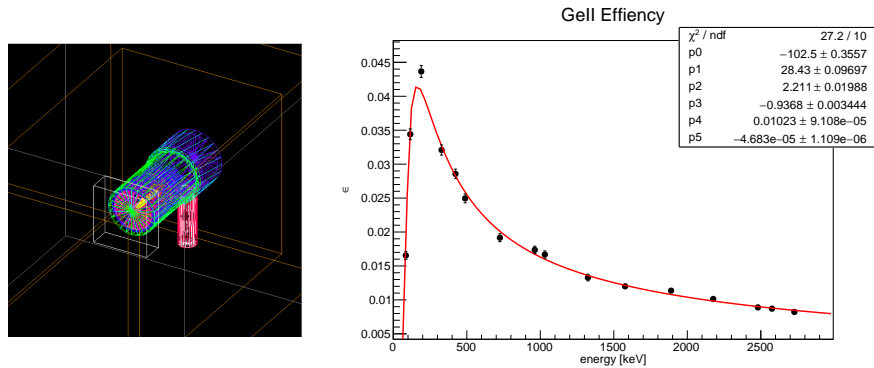


Figure 2: Sample geometry and HPGe detection efficiency ε vs energy E . $\varepsilon(E) = p_0 + p_1 \cdot \log(E) + p_2 \cdot \log^2(E) + p_3 \cdot \log^3(E) + p_4 \cdot \log^5(E) + p_5 \cdot \log^7(E)$

Counting rates were converted into nuclide-specific decay rates using energy-dependent detection efficiencies, determined by means of GEANT4 detector simulations, as described in [23]. The left panel of Figure 2 shows a rendering of the simulated geometry for the UA GeII setup. An example for an efficiency curve and a parametric fit to the Monte Carlo data is shown in the right panel of Figure 2.

An example of the observed in-growth of radon progeny and the time fits used to determine the transient and constant activity fractions is shown in Figure 3 for the A1 sample. ^{226}Ra was detected via the 186-keV peak, ^{214}Pb via the 295-keV and 352-keV lines, and ^{214}Bi via the 609-keV, 1120-keV, and 1764-keV peaks. γ -radiation with 186.2 and 185.7 keV is emitted in the decay of

^{226}Ra (^{238}U series) and ^{235}U , respectively. The resulting full absorption peaks cannot be resolved from each other. The determination of the ^{226}Ra activity accounts for this degeneracy, assuming ^{235}U and ^{238}U are present in the samples with their natural isotopic abundances. The solid lines show the time functions fit to the data. The constant, A_{ne} , and transient, A_e , ^{214}Pb and ^{214}Bi activity terms were determined by fitting the data with:

$$A(t) = A_{\text{ne}} + A_e \cdot \left(1 - e^{-t/\tau_{\text{Rn}}}\right) \quad (1)$$

with $\tau_{\text{Rn}} = 7943.2$ min denoting the mean life time of ^{222}Rn . A_e and A_{ne} are interpreted as the emanated and non-emanated ^{222}Rn progeny fractions. Assuming secular equilibrium and lossless radon collection, $A_{\text{Rn}} = A_e + A_{\text{ne}}$ is equal to the ^{222}Rn decay rate. The various peak activities were combined by means of a weighted average.

Note in Figure 3 that the ^{226}Ra activity, A_{Ra} , was found to be constant, as expected. The growth of the ^{214}Pb and ^{214}Bi activities follows the ^{222}Rn mean life time, also as expected. The other sample data behaves in a similar way. In order to study the ^{226}Ra - ^{222}Rn balance, Figure 4 shows the relative activity difference $\Delta = \frac{A_{\text{Ra}} - A_e - A_{\text{ne}}}{A_{\text{Ra}}}$ for the different dust sample measurements.

One would expect Δ to be compatible with zero in case all ^{222}Rn production and disappearance has been accounted for. The high points in Figure 4 correspond to measurements made with detector UA GeII, and the two low points to those made with JP Ge2. The plot shows a 10% upward bias for the UA GeII data and a 2% downward bias for the JP Ge2 points, relative to the average. We interpret this data to show that the radon production and disappearance is accounted for within 10% uncertainty. The average density of the dust and approximate bag sizes were used for the simulation of two HPGe detectors. This is an additional source of uncertainty. The reported out-gassing fractions take this uncertainty into account.

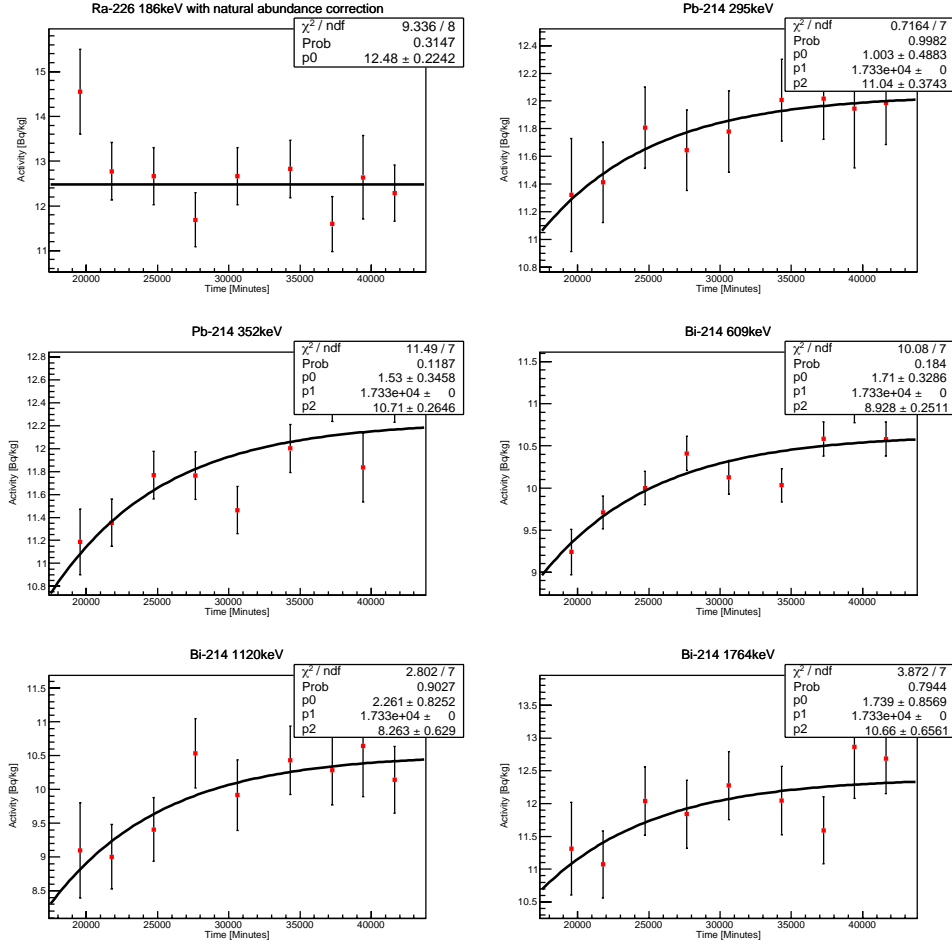


Figure 3: In-growth of emanated radon daughters observed for the dust sample from SURF SAL sweepings

4. Results and Discussion

The measured ^{226}Ra , emanated, non-emanated radon activities and emanation fractions are given in Table 3 for all samples. The measured radon emanation fractions, determined as $f = \frac{A_e}{A_e + A_{ne}}$ are given in Table 3 too. The stated emanation fractions were determined as the weighted average of the peak-wise emanation fractions. The error estimation for the f-values accounts for

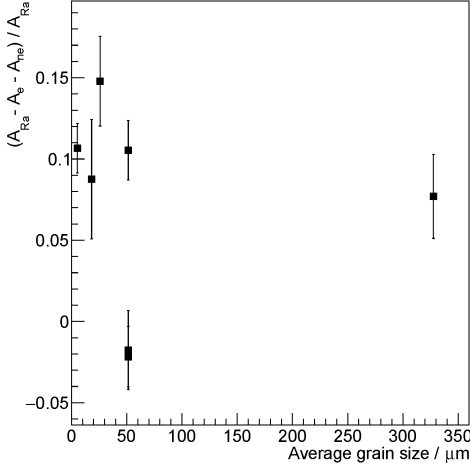


Figure 4: Relative difference Δ of the ^{226}Ra and ^{222}Rn activities as a function of average grain size.

the strong error anti-correlation observed for A_e and A_{ne} . The radon emanation fractions from dust observed in this study lie between $3.5 \pm 1.9\%$ and $16.1 \pm 0.84\%$, as shown in Table 3.

Figure 5 depicts the observed radon emanation fraction as a function of the average particle size. The initially expected overall anti-correlation of these fractions is not observed. When comparing similar samples, A-type with A-type and AFRL samples with the other AFRL sample, an anti-correlation is seen.

Comparing the emanation fraction measured for the dry A4 sample to that measured for the A4 sample exposed to moist air, they are equal to within statistical uncertainties. Hence, there is no clear evidence that exposure of the dust samples to ambient laboratory conditions affected the results.

Extensive modeling studies have been carried out and compared with data to understand the salient mechanisms and characteristics underlying radon emanation; for a recent comprehensive review of these studies, see Reference [24]. Radon emanation from a single grain is understood to be dominated by nuclear recoil from radium decay, although radon diffusion cannot be neglected

Sample	^{226}Ra activity [Bq/kg]	Emanated $^{214}\text{Pb} - ^{214}\text{Bi}$ activity [Bq/kg]	Non-emanated $^{214}\text{Pb} - ^{214}\text{Bi}$ activity [Bq/kg]	Emanation fraction
A1 Dust ($5.3 \pm 3.3 \mu\text{m}$)	46.9 ± 0.58	6.8 ± 0.41	35.1 ± 0.27	$16.1 \pm 0.84\%$
A4 Dust ($51.4 \pm 52.5 \mu\text{m}$)	29.1 ± 0.43	3.3 ± 0.31	22.8 ± 0.20	$12.7 \pm 1.1\%$
AFRL-02 Dust ($18.2 \pm 20.7 \mu\text{m}$)	4.9 ± 0.13	0.33 ± 0.11	4.2 ± 0.08	$7.3 \pm 2.2\%$
AFRL-03 Dust ($25.9 \pm 24.5 \mu\text{m}$)	6.6 ± 0.14	0.2 ± 0.11	5.4 ± 0.08	$3.5 \pm 1.9\%$
SURF SAL sweepings ($327.5 \pm 242.2 \mu\text{m}$)	12.5 ± 0.22	1.6 ± 0.20	10.0 ± 0.15	$13.6 \pm 1.53\%$
A4 Dust (Dry sample)	24.0 ± 0.37	2.7 ± 0.19	21.8 ± 0.14	$10.9 \pm 0.7\%$
A4 Dust (Moist sample)	23.8 ± 0.38	2.2 ± 0.37	22.1 ± 0.22	$8.9 \pm 1.4\%$

Table 3: ^{226}Ra activities, derived from the 186 keV peak, were corrected for the natural abundances of ^{235}U and ^{238}U . Statistical uncertainties are listed. A 10%/15% systematic uncertainty is assigned to the efficiency corrections of UA Ge2/JP Ge2.

at much higher temperatures. However, the range of temperatures much larger than room temperature is not relevant for most experiments worrying about radon emanation. The emanation fraction then further depends on the nuclear recoil range in the material, grain size, shape, and surface texture, pores in the grain, and the radium distribution within the grain. Whether or not an ejected radon atom survives to emerge from the dust, rather than becoming embedded in another grain, depends on the proximity and packing of neighboring grains. Moisture is another influential factor, acting to increase radon emanation, since radon is slowed much faster in water than air and thus less likely to become embedded in a neighboring grain.

Since our dust samples we measured are dry, we compare our results to modeling of radon emanation from dry dust. It should also be noted that although our dust samples were spread out in a loose thin layer for emanation, the layers were thick on the scale of any typical grain size. The dominating scenario

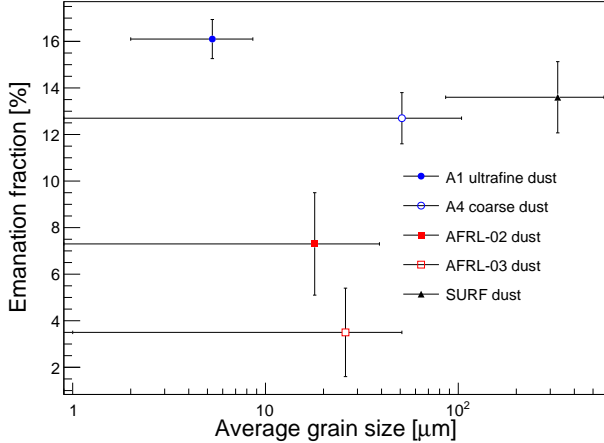


Figure 5: Observed emanation fractions versus average particle size. Blue points correspond to the A-type dust samples, points in red to AFRL-dust. The black point denotes the SURF sample. The vertical error bars correspond to the measurement uncertainty of the emanation fraction. The horizontal error bars indicate the standard deviations of the respective particle size distributions. The A4 data point corresponds to the weighted average of all measurements reported in Table 3.

would then seem to be emanation from single grains in the presence of neighboring grains rather than simple emanation from single grains. Modeling results for dusts comprised of submicron grains cannot be compared to our measurements as grain sizes in our samples are larger than 1 micron. Our measurements were carried out at ambient laboratory temperatures, so emanation due to diffusion of radon from the grains is taken to be negligible.

In comparing the emanation fractions of the commercial samples with the same composition but differing grain size distributions, the emanation factor for the A1 and A4 samples decreases markedly with increasing grain size; while for the AFRL-02 and AFRL-03 samples, the emanation factor decreases slightly with increasing average grain size and could be taken as the same within statistical uncertainties. Taking all 5 samples together, including the SURF laboratory sample, emanation fraction is obviously not dependent on grain size alone, and

in fact the sample with the largest emanation fraction is the sample comprised of the largest grains.

Modeling of emanation from single grains, where the grains are spherical or cylindrical in shape [25, 26] yield the expectation that emanation fraction does decrease as size increases. On the other hand, as already mentioned, we expect emanation in the presence of neighboring grains to have dominated for our samples. For this scenario, modeling assuming spherical grains of uniform radius predicts that emanation fractions for dry dusts should increase rapidly with grain size over the range 1-100 μm [27, 28]. Multigrain models can yield predictions of nearly constant or decreasing emanation fraction with increasing grain size in the case that the radium distribution is assumed to be uniform throughout the grain, but then the magnitude of the emanation fraction is orders of magnitude lower than observed [28]. In any case, multigrain models assuming spherical grains could well be invalid at least for the A1 and A4 samples, where shape measurements indicate that the grain shapes deviate significantly from spherical on the whole. Another multigrain model [29], developed to explain emanation from soils, is able to reproduce the trend of decreasing fraction with increasing grain size by taking smaller grains to have larger specific areas.

In summary, it is not clear that any model investigated so far yields predictions which broadly agree with our results for emanation dependence on grain size for samples of the same composition. Agreement may be substantially improved, at least for the A1 and A4 samples, if the knowledge of the grain shape is taken accurately into account. Comparison of calculations we have done between spherical and oblatel spheroidal grain shapes shows that the radon emanation fraction is a factor of 4 larger for oblate spheroids having an equatorial diameter eight times greater than the polar diameter. This demonstrates the importance of the knowledge on the shape of the grains. Supposing that the deviation of grain shape from spherical is a strong influence on the observed emanation fractions, any future measurement of dust shape and surface texture for the AFRL-02 and AFRL-03 dust samples could be incorporated into mod-

eling emanation fractions for these dusts and compared with our observations. Finally, gaining insight into the observed emanation fraction for the SURF dust would be facilitated by measuring its composition as well as the shapes of its grains, a future project we are considering to undertake.

5. Acknowledgements

This work was conceived as a contribution to the construction of the LZ experiment. We thank our LZ colleagues for their support. We are especially grateful to Al Smith and Kevin Lesko of Lawrence Berkeley National Laboratory (LBNL) for bringing the radon progeny time method to our attention. We thank Bettersize Instruments Ltd to their help in measuring the particle size distributions. This research was supported in part by the U.S. Department of Energy under DOE Grant DE-SC0012447, by a grant from the National Science Foundation of China (No. 12005131), Shanghai Pujiang Program (No.19PJ1405800) and a grant from Sichuan Science and Technology Program (No.2020YFSY0057).

References

- [1] J. Aalbers, et al., Darwin: towards the ultimate dark matter detector, *Journal of Cosmology and Astroparticle Physics* 2016 (11) (2016) 017–017. [arXiv:1606.07001](https://arxiv.org/abs/1606.07001), doi:10.1088/1475-7516/2016/11/017.
- [2] D. S. Akerib, et al., Results from a search for dark matter in the complete LUX exposure, *Phys. Rev. Lett.* 118 (2) (2017) 021303. [arXiv:1608.07648](https://arxiv.org/abs/1608.07648), doi:10.1103/PhysRevLett.118.021303.
- [3] E. Aprile, et al., Dark Matter Search Results from a One Ton-Year Exposure of XENON1T, *Phys. Rev. Lett.* 121 (11) (2018) 111302. [arXiv:1805.12562](https://arxiv.org/abs/1805.12562), doi:10.1103/PhysRevLett.121.111302.
- [4] G. Anton, et al., Search for neutrinoless double- β decay with the complete exo-200 dataset, *Phys. Rev. Lett.* 123 (2019) 161802. [arXiv:1906.02723](https://arxiv.org/abs/1906.02723), doi:10.1103/PhysRevLett.123.161802.
- [5] The CUPID Interest Group, CUPID pre-CDR (2019). [arXiv:1907.09376](https://arxiv.org/abs/1907.09376).
- [6] D. S. Akerib, et al., The LUX-ZEPLIN (LZ) Experiment, *Nucl. Instrum. Meth. A* 953 (2020) 163047. [arXiv:1910.09124](https://arxiv.org/abs/1910.09124), doi:10.1016/j.nima.2019.163047.
- [7] Q. Wang, et al., Results of dark matter search using the full PandaX-II exposure, *Chin. Phys. C* 44 (12) (2020) 125001. doi:10.1088/1674-1137/abb658.
- [8] E. Aprile, et al., Projected WIMP sensitivity of the XENONnT dark matter experiment, *JCAP* 11 (2020) 031. [arXiv:2007.08796](https://arxiv.org/abs/2007.08796), doi:10.1088/1475-7516/2020/11/031.
- [9] E. Armengaud, et al., New Limit for Neutrinoless Double-Beta Decay of ^{100}Mo from the CUPID-Mo Experiment, *Phys. Rev. Lett.* 126 (2021) 181802. [arXiv:2011.13243](https://arxiv.org/abs/2011.13243), doi:10.1103/PhysRevLett.126.181802.

- [10] G. Adhikari, et al., nEXO: neutrinoless double beta decay search beyond 10^{28} year half-life sensitivity, *J. Phys. G: Nucl. Part. Phys.* 49 (2022) 015104. [arXiv:2106.16243](https://arxiv.org/abs/2106.16243), doi:10.1088/1361-6471/ac3631.
- [11] N. Abgrall, et al., LEGEND-1000 preconceptual design report (2021). [arXiv:2107.11462](https://arxiv.org/abs/2107.11462).
- [12] Y. Meng, et al., Dark Matter Search Results from the PandaX-4T Commissioning Run (7 2021). [arXiv:2107.13438](https://arxiv.org/abs/2107.13438).
- [13] A. I. Amasi, K. M. Mtei, C. N. Dinh, P. Jodlowski, Radon mass exhalation rates of selected building materials in Tanzania, *Journal of Environment and Earth Science* 5 (21) (2015) 57–63.
- [14] R. Kumaria, K. Kanta, M. Garg, The effect of grain size on radon exhalation rate in natural-dust and stone-dust samples, *Physics Procedia* 80 (2015) 128–130.
- [15] C. Cameron, A review of radon emanation and mobilization in minerals and rocks, *Tech. Rep. MP GL-87-27*, University of Southern Mississippi/U.S. Army Corp of Engineers (1987).
- [16] Y. I. et al., Measurement and calculation of radon releases from norm residues, *Tech. Rep. Series 474*, International Atomic Energy Agency (2013).
- [17] W. Nazaroff, A. Nero, Jr, Radon and its decay products in indoor air, John Wiley & Sons, New York, Chichester, Brisbane, Toronto, Singapore, 1988. URL <https://www.osti.gov/biblio/6907171>
- [18] R. A. Fletcher, D. S. Bright, Shape factors of iso 12103-a3 (medium test dust), *Filtration & Separation* 37 (2000) 48–56.
- [19] X. Woodward, A. Kostinski, S. China, C. Mazzoleni, W. Cantrell, Characterization of dust particles' 3d shape and roughness with nanometer

resolution, *Aerosol Science and Technology* 49 (4) (2015) 229–238. doi:10.1080/02786826.2015.1017550.

[20] C. Wagner, F. Hanisch, N. Holmes, H. de Coninck, G. Schuster, J. N. Crowley, The interaction of n_{205} with mineral dust: aerosol flow tube and knudsen reactor studies, *Atmospheric Chemistry and Physics* 8 (1) (2008) 91–109. doi:10.5194/acp-8-91-2008.
URL <https://acp.copernicus.org/articles/8/91/2008/>

[21] B. J. Connolly, E. Loth, C. F. Smith, Shape and drag of irregular angular particles and test dust, *Powder Technology* 363 (2020) 275–285. doi:<https://doi.org/10.1016/j.powtec.2019.12.045>.
URL <https://www.sciencedirect.com/science/article/pii/S0032591019311519>

[22] Y. Meng, J. Busenitz, A. Piepke, A new method for evaluating the effectiveness of plastic packaging against radon penetration, *Applied Radiation and Isotopes* 156 (2020) 108963. doi:<https://doi.org/10.1016/j.apradiso.2019.108963>.

[23] R. Tsang, A. Piepke, D. Auty, B. Cleveland, S. Delaquis, T. Didberidze, R. MacLellan, Y. Meng, O. Nusair and T. Tolba, GEANT4 models of HPGe detectors for radioassay, *Nuclear Instruments and Methods in Physics Research Section A: Accelerators, Spectrometers, Detectors and Associated Equipment* 935 (2019) 75 – 82. doi:10.1016/j.nima.2019.04.085.

[24] A. Sakoda, Y. Ishimori, Mechanisms and modeling approaches of radon emanation for natural materials, *Japanese Journal of Health Physics* 52 (2017) 296–306.

[25] R. L. Fleischer, Theory of alpha recoil effects on radon release and isotopic disequilibrium, *Geochimica et Cosmochimica Acta* 47 (4) (1983) 779–784. doi:[https://doi.org/10.1016/0016-7037\(83\)90111-4](https://doi.org/10.1016/0016-7037(83)90111-4).
URL <https://www.sciencedirect.com/science/article/pii/0016703783901114>

[26] T. M. Semkow, Recoil-emanation theory applied to radon release from mineral grains, *Geochimica et Cosmochimica Acta* 54 (2) (1990) 425–440. doi:[https://doi.org/10.1016/0016-7037\(90\)90331-E](https://doi.org/10.1016/0016-7037(90)90331-E).
URL <https://www.sciencedirect.com/science/article/pii/001670379090331E>

[27] Experimental and modeling studies of grain size and moisture content effects on radon emanation, *Radiation Measurements* 45 (2) (2010) 204–210. doi:<https://doi.org/10.1016/j.radmeas.2010.01.010>.
URL <https://www.sciencedirect.com/science/article/pii/S1350448710000119>

[28] J. Stajic, D. Nikezic, Theoretical calculation of radon emanation fraction, *Nuclear Instruments and Methods in Physics Research Section B: Beam Interactions with Materials and Atoms* 336 (2014) 19–25. doi:<https://doi.org/10.1016/j.nimb.2014.06.013>.
URL <https://www.sciencedirect.com/science/article/pii/S0168583X14006132>

[29] N. Chitra, S. B. Sundar, I. I. Valan, V. Subramanian, M. T. Jose, B. Venkatakrishnan, MODELING AND EXPERIMENTS TO ESTIMATE RADON EMANATION FACTOR IN SOIL—GRAIN SIZE AND MOISTURE EFFECT, *Radiation Protection Dosimetry* 194 (2-3) (2021) 104–112.